# Experimental realization of strange nonchaotic attractors in a quasiperiodically forced electronic circuit

K. Thamilmaran[1], D. V. Senthilkumar[1], A. Venkatesan[2], and M. Lakshmanan[1*]

[1] *Centre for Nonlinear Dynamics, Department of Physics, Bharathidasan University, Tiruchirapalli - 620 024, India*

*and*

[2] *Department of Physics, Nehru Memorial College, Puthanampatti - P.O, Tiruchirappalli - 621 007, India*



(Dated: February 7, 2008)

## Abstract

We have identified the three prominent routes, namely Heagy-Hammel, fractalization and intermittency routes, and their mechanisms for the birth of strange nonchaotic attractors (SNAs) in a quasiperiodically forced electronic system constructed using a negative conductance series LCR circuit with a diode both numerically and experimentally. The birth of SNAs by these three routes is verified from both experimental and their corresponding numerical data by maximal Lyapunov exponents, and their variance, Poincaré maps, Fourier amplitude spectrum, spectral distribution function and finite-time Lyapunov exponents. Although these three routes have been identified numerically in different dynamical systems, the experimental observation of all these mechanisms is reported for the first time to our knowledge and that too in a single second order electronic circuit.

PACS numbers: 05.45.+b

*Electronic address: lakshman@cnld.bdu.ac.in

## I. INTRODUCTION

Strange nonchaotic attractors are regarded as structures in between regularity and chaos. They are geometrically strange as evidenced by their fractal nature, which is common to all chaotic systems. However, they are nonchaotic in a dynamical sense because they do not show sensitivity with respect to changes in initial conditions (as evidenced by negative Lyapunov exponents), just like, regular systems. Following the initial study of Grebogi et al. [1], several theoretical as well as experimental studies have been made pertaining to the existence and characterization of SNAs in different quasiperiodically driven nonlinear dynamical systems. In particular the SNAs have been reported to arise in many physically relevant situations such as the quasiperiodically forced pendulum [2], the quantum particles in quasiperiodic potentials [3], biological oscillators [4], the quasiperiodically driven Duffing-type oscillators [5, 6, 7, 8], velocity dependent oscillators [9], electronic circuits [10, 11, 12] and in certain maps [13, 14, 15, 16, 17, 18, 19, 20, 21, 22]. Also, these exotic attractors were confirmed by an experiment consisting of a quasiperiodically forced, buckled, magneto-elastic ribbon [23], in analog simulations of a multistable potential [24], and in a neon glow discharge experiment [25]. The SNAs are also related to the Anderson localization in the Schrödinger equation with a quasiperiodic potential [26, 27] and they may have a practical application in secure communication [28, 29, 30].

The existence of SNAs in the above physically relevant systems has naturally motivated further intense investigations on their nature and occurrence. A question of intense further interest is the way in which they arise and ultimately become chaotic. In this context, several routes have been identified in recent times and for a few of them typical mechanisms have been found for the creation of SNAs. The major routes by which the SNAs appear may be broadly classified as follows: torus doubling route to chaos via SNAs [22], gradual fractalization of torus [17], the appearance of SNAs via blowout bifurcation [6], the occurrence of SNAs through intermittent phenomenon [12, 13, 19, 20, 21, 31], the formation of SNAs via homoclinic collision [27], remerging of torus doubling bifurcations and the birth of SNAs [9], the existence of SNAs in the transition from two-frequency to three-frequency quasiperiodicity [7], the transition from three-frequency quasiperiodicity to chaos via a SNA [4] and the transition to chaos via strange nonchaotic trajectories on the torus [32]. Different mechanisms have been identified for some of the above routes, which are summarised in Table I.

TABLE I: Routes and mechanisms of the onset of various SNAs

| **Type of route** | **Mechanism** |
|---|---|
| Heagy-Hammel [22] | Collision of period-doubled torus with its unstable parent |
| Gradual Fractilization [17] | Increased wrinkling of torus without any interaction with nearby periodic orbits |
| On-off intermittency [6] | Loss of transverse stability of torus |
| Type-I intermittency [13] | Due to saddle-node bifurcation, a torus is replaced by SNA |
| Type-III intermittency [12] | Subharmonic instability |
| Homoclinic collision [27] | Homoclinic collisions of the quasiperiodic orbits |

Among these various routes/mechanisms for the birth of SNAs, the Heagy-Hammel, the gradual fractalization and the intermittency routes/mechanisms to SNAs are quite general and very robust to observe in a number of quasiperiodically forced nonlinear dynamical systems. So far, these dynamical transitions are identified only through numerical analysis in different dynamical systems, prominent among being discrete and continuous flow systems. Eventhough there exist various experimental realizations of SNAs in physical systems [23, 24, 25], the genesis of SNAs through different routes/mechanisms have not yet been reported experimentally to the best of our knowledge, except for type-III intermittent route by two of the present authors and K. Murali [12]. In view of this fact, in the present work, we consider a simple nonlinear electronic circuit system, a second-order dissipative nonautonomous negative conductance series LCR circuit, and investigate the dynamics of the circuit under quasiperiodic forcing. We have identified that the circuit exhibits the three familiar dynamical transitions, namely Heagy-Hammel, fractalization and intermittency transitions involving SNAs. Further, the dynamical transitions are characterized from both experimental and their corresponding numerical data by the maximal Lyapunov exponents, and their variance, Poincaré maps, Fourier amplitude spectrum, spectral distribution function and finite-time Lyapunov exponents. We believe that this is the first experimental

demonstration of the existence of all the three prominent routes/mechanisms to SNA and that too in a simple single electronic circuit to the best of our knowledge.

The paper is organized as follows. In Sec. II, we present a brief introduction of the experimental realization of the quasiperiodically forced negative conductance series LCR circuit with diode. In Sec. III, we describe the phase diagram for the circuit where the regions corresponding to the different dynamical behaviors are delineated as a function of parameters based on numerical analysis. Section IV is devoted to the computer simulation studies and experimental confirmation of the creation of strange nonchaotic attractors via Heagy-Hammel route while in Sec. V the creation of SNAs through gradual fractalization is studied both numerically and experimentally. In Sec. VI, the type-I intermittent route to SNA is shown to exist both numerically and experimentally. Finally, in Sec. VII, we summarize our results.

## II. CIRCUIT REALIZATION

We consider here the simple second-order nonlinear dissipative nonautonomous negative conductance series LCR circuit with a single voltage generator introduced by us very recently [33] and shown in Fig. 1(a). The circuit consists of a series LCR network, forced by two sinusoidal voltage generators $f_1(t)$ and $f_2(t)$ (HP 33120A series). Two extra components, namely a *p-n junction* diode (D) and a linear negative conductor $g_N$, are connected in parallel to the forced series LCR circuit. The negative conductor used here is a standard op-amp based negative impedance converter (NIC). The diode operates as a nonlinear conductance, limiting the amplitude of the oscillator. In the Fig. 1(a), $v, i_L$ and $i_D$ denote the voltage across the capacitor $C$, the current through the inductor $L$ and the current through the diode $D$, respectively. The actual $v - i$ characteristic of the diode (given by Fig. 1(b)) is approximated by the usual two segment piecewise-linear function (see Fig. 1(c)) which facilitates numerical analysis considerably. The state equations governing the presently proposed circuit given in Fig. 1 are a set of two first-order nonautonomous differential equations:

$$C\frac{dv}{dt} = i_L - i_D + g_N v, \tag{1a}$$

$$L\frac{di_L}{dt} = -Ri_L - v + E_{f1}\sin(\omega_{f1}t) + E_{f2}\sin(\omega_{f2}t). \tag{1b}$$

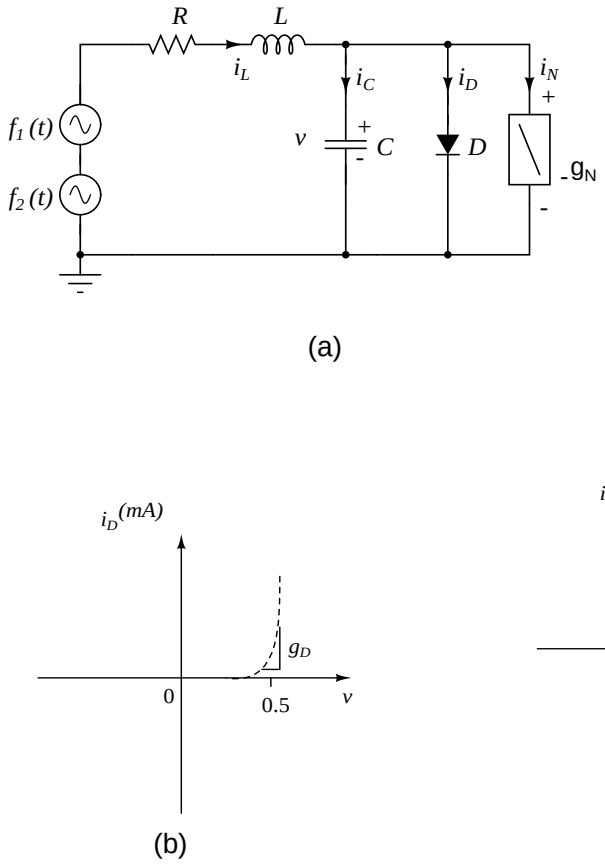


FIG. 1: (a) Circuit realization of a simple nonautonomous circuit. Here, $D$ is the *p-n junction* diode, and $g_N$ is negative conductance. The parameter values of the other elements are fixed as $L = 50.0\ mH$, $C = 10.32\ nF$. The external emf $f_1(t) = E_{f1} \sin \omega_{f1} t$ and $f_2(t) = E_{f2} \sin \omega_{f2} t$ are the function generators ($HP\ 33120A$). The values of $\omega_{f1}$ and $\omega_{f2}$ are chosen as 5982.0 $Hz$ and 13533.0 $Hz$ respectively. The forcing amplitude $E_{f2}$ is fixed as 0.15 $V$. The other forcing amplitude $E_{f1}$ and the resistance $R$ are taken as control parameters which are being varied in our analysis, (b) $i - v$ characteristics of the *p-n junction* diode and (c) two segment piecewise-linear function.

Here,

$$i_D(v) = \begin{cases} g_D(v - V), & v \geq V, \\ 0, & v < V, \end{cases} \tag{1c}$$

where $g_D$ is the slope of the characteristic curve of the diode, $E_{f1}$ and $E_{f2}$ are the amplitudes and $\omega_{f1}$ and $\omega_{f2}$ are the angular frequencies of the forcing functions $f_1(t) = E_{f1} \sin \omega_{f1} t$ and $f_2(t) = E_{f2} \sin \omega_{f2} t$, respectively. In the absence of $E_{f2}$, the circuit (Fig. 1(a)) has

been shown to exhibit chaos and also strong chaos not only through the familiar period-doubling route but also via torus breakdown followed by period-doubling bifurcations [33]. In order to construct the actual experimental circuit, the numerical simulation is used to determine the correct parametric values for observing strange nonchaotic attractor. The values of diode conductance $g_D$, negative conductance $g_N$ and break voltage $V$ are fixed as 1313 $\mu S$, $-0.45$ $mS$, and 0.5 $V$ respectively. After some trial and error, we chose the actual experimental values of the inductance, $L$, capacitance, $C$ and external frequencies $\omega_{f1}$ and $\omega_{f2}$ as 50 $mH$, 10.32 $nF$, 5892 $Hz$ and 13533 $Hz$.

In order to study the dynamics of the circuit in detail, Eq. (1) can be converted into a convenient normalized form for numerical analysis by using the the following rescaled variables and parameters $\tau = t/\sqrt{LC}$, $x = v/V$, $y = (i_L/V)(\sqrt{(}LC)$, $E_1 = E_{f1}/V$, $E_2 = E_{f2}/V$, $\omega_1 = \omega_{f1}\sqrt{(}LC)$, $\omega_2 = \omega_{f2}\sqrt{(}LC)$, $a = R\sqrt{(}C/L)$, $b = g_N\sqrt{(}L/C)$, and $c = g_D\sqrt{(}L/C)$.
The normalized evolution equation so obtained is

$$\begin{aligned}
\dot{x} &= y + f(x), \\
\dot{y} &= -x - ay + E_1 \sin(\theta) + E_2 \sin(\phi), \\
\dot{\theta} &= \omega_1, \\
\dot{\phi} &= \omega_2,
\end{aligned} \tag{2a}$$

where

$$f(x) = \begin{cases} (b-c)x + c, & x \geq 1, \\ bx, & x < 1. \end{cases} \tag{2b}$$

Here dot stands for the differentiation with respect to $\tau$.

The dynamics of Eq. (2) now depends on the parameters $a$, $b$, $c$, $\omega_1$, $\omega_2$, $E_1$ and $E_2$. The rescaled parameters correspond to the values $b = 0.99051$, $c = 2.89$, $\omega_1 = 0.133841$, $\omega_2 = 0.307411$ and $E_2 = 0.3$. The amplitude of external quasiperiodic forcing $E_1$ and the value of $a$ (or equivalently $E_{f1}$ and $R$ in Eq. (1)) are taken as control parameters which are being varied in our numerical (and experimental) studies.

## III. TWO PARAMETER PHASE DIAGRAM

To be concrete, we first consider the dynamics of the system (2) and numerically integrate it. Using various characteristic quantities such as Lyapunov exponents, power spectral measures and distribution of finite-time Lyapunov exponents, we distinguish periodic, quasiperiodic, strange nonchaotic and chaotic attractors. In particular, the Poincaré surface of section plot in the $(\phi - x)$ plane with $\phi$ modulo $2\pi$ can clearly indicate whether an attractor possesses a geometrically smooth or complicated structure. However, the estimation of the Lyapunov exponents for this attractor(that is positive or negative value including zero) as well as its variance will identify whether it is a chaotic or nonchaotic one. In addition to the fact that the Lyapunov exponents are negative for SNAs, the variance - the fluctuations in the measured value of the Lyapunov exponents on SNAs - is also found to be large. Finer distinction among SNAs formed via different mechanisms can be made by analyzing the nature of the variation of Lyapunov exponents and its variance near the transition values of the control parameters. Then we experimentally confirm the results for circuit Eq. (1) geometrically by observing the phase trajectory and the power spectrum. For our experimental study of the circuit given in Fig. 1, a two dimensional projection of the attractor is obtained by measuring the voltage $v$ across the capacitor $C$ and the current $i_L$ through the inductor $L$ and connected to the $X$ and $Y$ channels of an oscilloscope. The phase trajectory obtained in the experiment is compared with the numerical trajectory. Then, a live picture of the corresponding power spectrum (obtained from a digital storage oscilloscope - HP 54600 series) of the projected attractor has also been used to distinguish the different attractors. In particular, to quantify the changes in the power spectrum obtained by numerically and experimentally, we compute the so-called spectral distribution function $N(\sigma)$,which is defined to be the number of peaks in the Fourier amplitude spectrum larger than some value, say $\sigma$. Scaling relations have been identified in the form $N(\sigma)$=$\log_{10}(1/\sigma)$ for the case of two-frequency quasiperiodic attractors and $N(\sigma) = \sigma^{-\beta}$, $1 < \beta < 2$, for the strange nonchaotic attractors.

Further to identify the different attractors in the two-parameter plane the dynamical transitions are traced out by two scanning procedures, both numerically and experimentally: (1) varying $E_1$(or $E_{f1}$) at fixed $a$ (= $R\sqrt{(}C/L)$, and (2) varying $a$ (or = $R$) at fixed $E_1$(or $E_{f1}/V$) in a 1000 X 1000 grid. The resulting phase diagram in the $(a - E_1)$ parameters

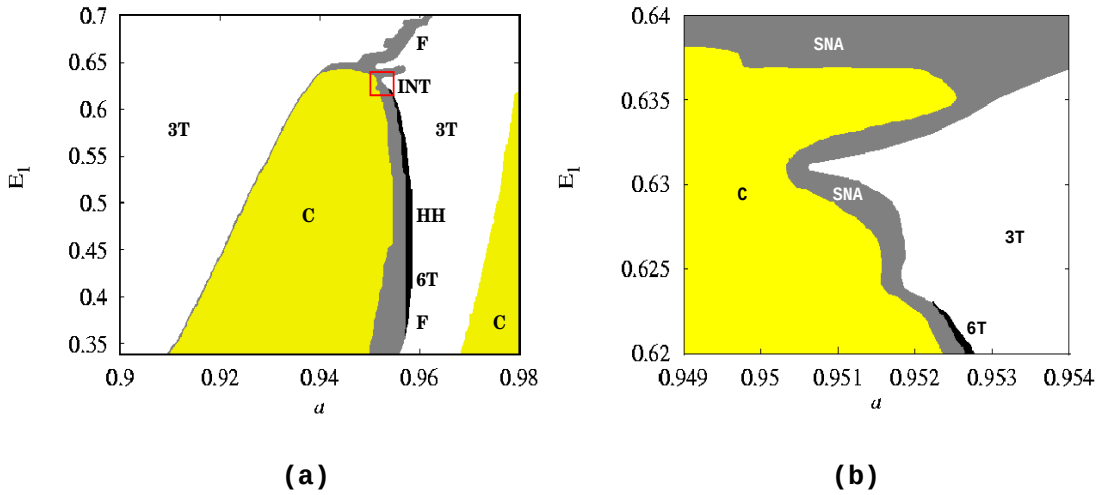


FIG. 2: (Color online)(a) Phase diagram in the $(a - E_1)$ plane for the circuit given in Fig. 1, represented by Eq. (2) and obtained from numerical data. 3T and 6T correspond to torus of period-3 and period-6 attractors, respectively. F, HH and INT denote the formation of SNAs through gradual fractalization, Heagy-Hammel and intermittency routes, respectively. C corresponds to chaotic attractor. (b) An enlarged version of the intermittent region indicated in (a).

space in the region $a \in (0.9,\ 0.98)$ and $E_1 \in (0.34,\ 0.7)$ is shown in Fig. 2 which has also been verified in the corresponding $(R - E_{f1})$ experimental parameter space. The various features indicated in the phase diagram are summarized and the main interesting features of the dynamical transitions are elucidated in the following.

Transitions from the right to left lower down in the $(a, E_1)$ space, through fractalization of the period-3 (3T) quasiperiodic attractors to SNA and then to chaos, occur for $0.953 < a < 0.955$ and $0.35 < E_1 < 0.37$. It is denoted as **F** in Fig. 2.

Moving from right to left in the middle region, one finds a torus doubling bifurcation from a period-3 torus (3T) to a period-6 (6T) quasiperiodic attractor and then to SNA via the Heagy-Hammel(HH) mechanism. This transition occurs in the range $0.953 < a < 0.958$ and $0.38 < E_1 < 0.58$. It is denoted as **HH** in Fig. 2.

Moving higher up in the amplitude space and from right to left, we find that SNAs and eventually chaos occur from period three-quasiperiodic attractor via type I intermittency route as $a$ is varied in the narrow range $0.949 < a < 0.954$ and for $E_1$ in the range $0.623 < E_1 < 0.645$. It is denoted as **INT** within a small box [Fig. 2(a)]. In Fig. 2(b), the enlarged portion of the box in Fig. 2(a) shows the region of existence of the intermittent

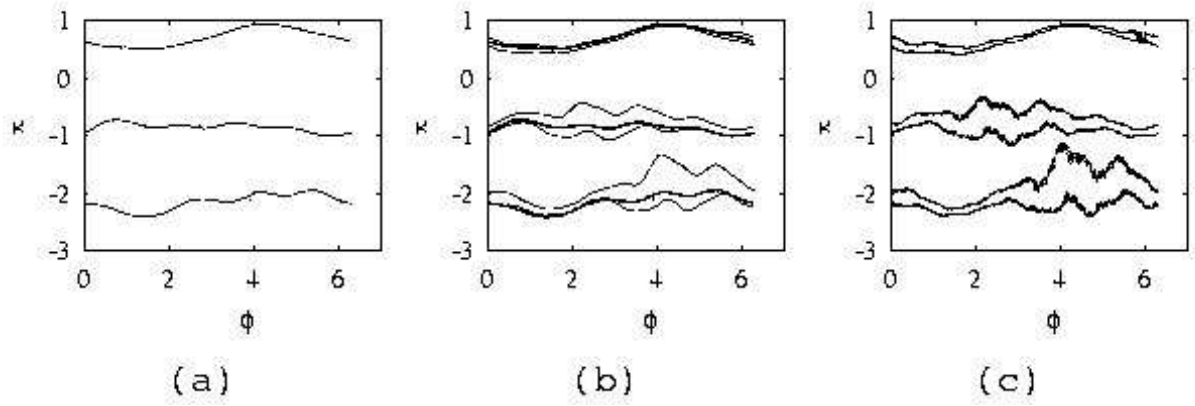


FIG. 3: Projection of the numerically simulated attractors of Eqs. (2) in the $(\phi - x)$ plane for fixed $E_1$ =0.44 and various values of $a$ indicating the transition from quasiperiodic attractor to SNA through Heagy-Hammel mechanism: (a) period-3 torus (3T) for $a$=0.95632, (b) period-6 torus (6T) for $a$=0.95593, and (c) SNA at $a$=0.95592.

SNA occuring between quasiperiodic and chaotic attractors.

In this section, we have identified atleast three interesting dynamical features namely, (1) Heagy-Hammel, (2) fractalization and (3) type I intermittent routes in the two-parameter diagram. Now, we describe each one of the them in detail from the point of view of numrical analysis as well as experimental identification as follows.

## IV. HEAGY-HAMMEL ROUTE TO SNA

The first of these routes that we encounter is the Heagy-Hammel route in which a period$-2^k$ torus gets wrinkled and upon collision with its unstable parent period$-2^{k-1}$ torus bifurcates into a SNA. Such a behavior has been observed in the present quasiperiodically forced negative conductance series LCR circuit within the range of $a$ values, $0.953 < a < 0.958$, and $E_1$ values, $0.38 < E_1 < 0.58$, while the other parameters are fixed as prescribed earlier in section II.

### A. Numerical Analysis

More specifically, let us fix the parameter $E_1$ at $E_1 = 0.44$, while decreasing the value of $a$. For $a = 0.95632$, the circuit equation (2) associated with Fig. 1 is found to exhibit a

period-3 torus attractor denoted as 3T (see Fig. 2) and the Poincaré map has three smooth branches (Fig. 3(a)), whose phase portrait and power spectrum are shown in Figs. 4a(i) and 4a(ii). As the value of $a$ is decreased to $a = 0.95593$, the attractor undergoes torus doubling bifurcation and the corresponding period-6 quasiperiodic orbit is denoted as 6T in Fig. 2 and the Poincaré map has six smooth branches as seen in Fig. 3(b). The corresponding phase portrait and power spectrum are shown in Figs. 4b(i) and 4b(ii). In the generic case, the period-doubling occurs in an infinite sequence until the accumulation point is reached, beyond which chaotic behavior appears. However, with tori, in the present case, further torus doubling does not takes place, but the torus becomes wrinkled; that is the truncation of the three torus doubling begins when the six strands of the 6T attractor become extremely wrinkled. This is because the period-doubled six torus collides with its unstable parent, and this occurs only for a few narrow selected parameter intervals, when $a$ is decreased to $a = 0.95593$ as shown in Fig.3(b). For example, when the value of $a$ is decreased to $a = 0.95592$, the attractor becomes extremely wrinkled. During this transition, the strands are seen to come closer to the unstable period 3T orbit and lose their continuities when the strands of torus doubled orbit collide with unstable parent and ultimately result in a fractal phenomenon as shown in Fig. 3(c) when $a$ is decreased to $a = 0.95592$. The phase portrait and power spectrum corresponding to Fig. 3(c) are shown in Figs. 4c(i) and 4c(ii). At such a value, the attractor, Fig. 3(c), possesses a geometrically strange property but does not exhibit sensitivity to initial conditions [the maximal Lyapunov exponent is negative as seen in Fig. 5(a)] and so it is indeed a strange nonchaotic attractor. As $a$ is decreased further to $a = 0.95435$, the attractor has eventually a positive Lyapunov exponent and hence it corresponds to chaotic attractor (denoted C in Fig. 2).

Now we examine the Lyapunov exponent for the transition from period-3 torus doubling to SNA. During this transition, the largest maximal Lyapunov exponent $\Lambda$ as a function of $a$ for a fixed $E_1 = 0.44$ remains negative, which is shown in Fig. 5(a). Hence, the attractor is strange but nonchaotic. We also note that there is an abrupt change in the maximal Lyapunov exponent during the transition from period-3 torus doubled attractor to SNA and its variance (Fig. 5(a) & 5(b)). When we examine this in a sufficiently small neighborhood of the critical value $a_{HH}$ =0.95593, the transition is clearly revealed by the Lyapunov exponent which varies smoothly in the torus region ($a < a_{HH}$) while it varies irregularly in the SNA region ($a > a_{HH}$). It is also possible to identify this transition point by examining the

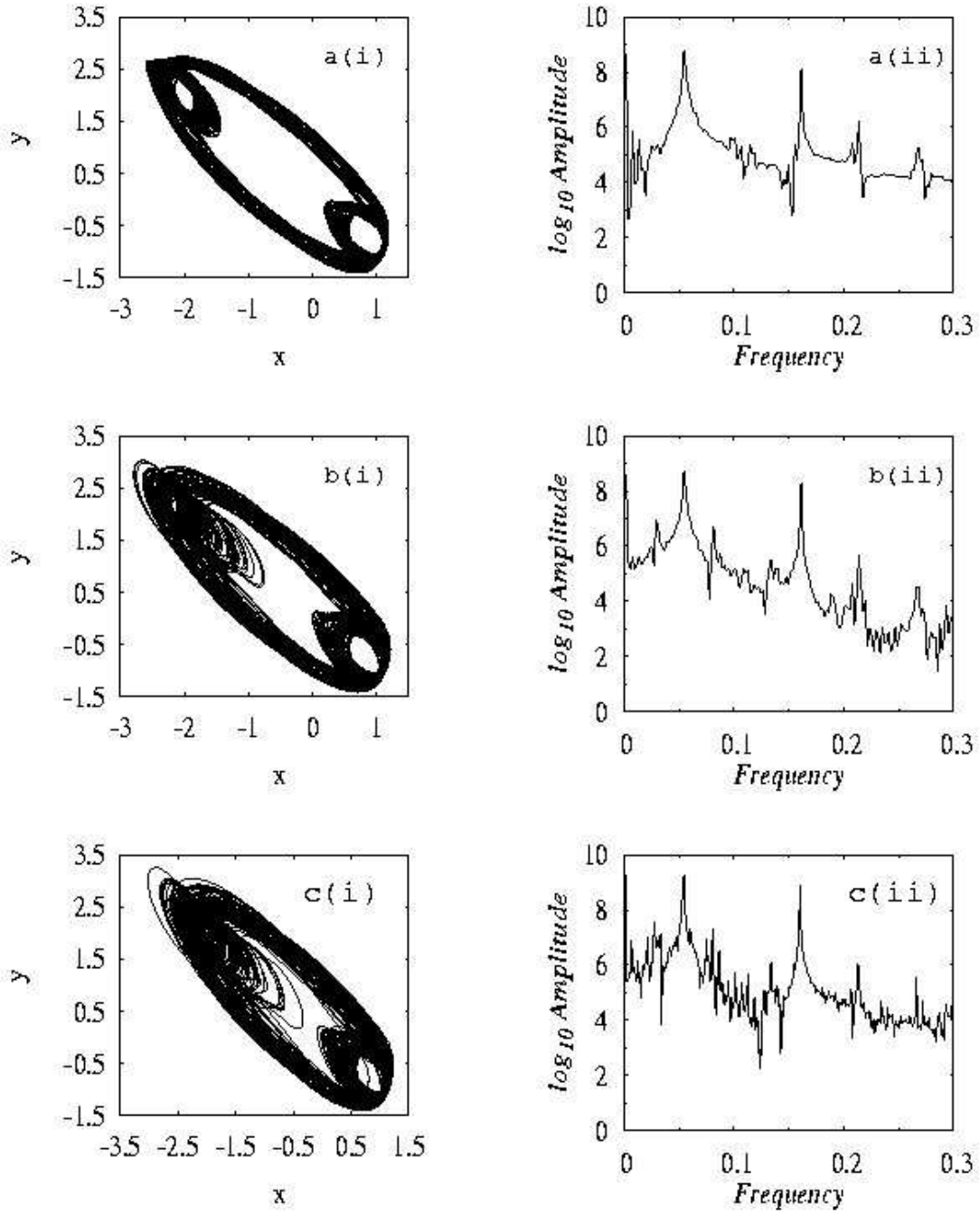


FIG. 4: Projection of the numerically simulated attractors of Eqs. (2) in the $(x, y)$ plane for fixed $E_1$ =0.44 and various values of $a$ indicating the transition from quasiperiodic attractor to SNA through Heagy-Hammel route: (a) period-3 torus (3T) for $a$=0.95632, (b) period-6 torus (6T) for $a$=0.95593 and (c) SNA at $a$=0.95592: (i) phase trajectory in the $(x - y)$ space; (ii) power spectrum.

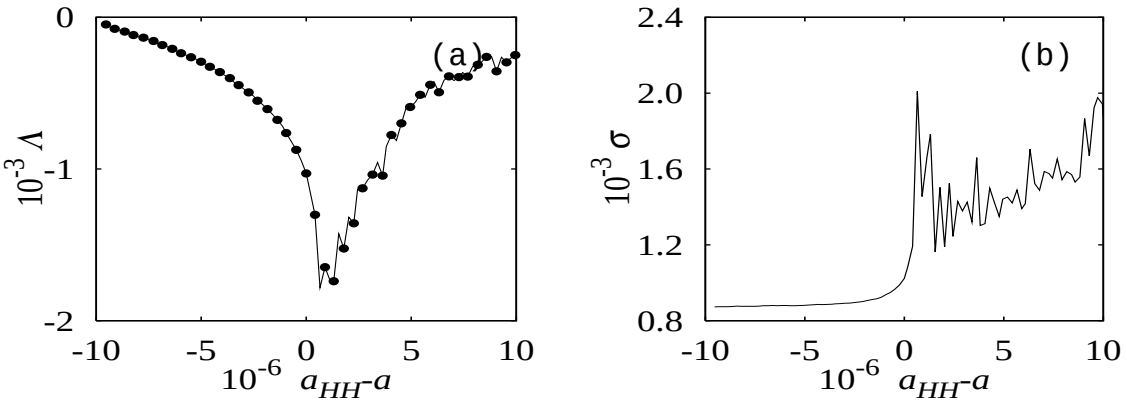


FIG. 5: Transition from three doubled torus to SNA through Heagy-Hammel route in region HH obtained from numerical data: (a) the behavior of the maximal Lyapunov exponent ($\Lambda$) and (b) the variance ($\sigma$) for $E_1$ =0.44.

variance of Lyapunov exponent, as shown in Fig. 5(b) in which the fluctuation is small in the torus region while it is large in the SNA region.

### B. Experimental Confirmation

To confirm that the above results hold good in the actual experimental circuits (Fig. 1) also, the phase trajectory is obtained experimentally by measuring the voltage $v$ across the capacitor $C$ and the current $i_L$ through the inductor $L$ in the circuit (Fig. 1) and connecting them to the $X$ and $Y$ channels of an oscilloscope. Then, a live picture of the corresponding power spectrum (obtained from a digital storage oscilloscope - HP 54600 series) of the projected attractor has also been used to distinguish the different attractors. The experimentally measured phase portraits and Fourier spectra shown in Figs. 6 correspond to the transition from period-3 torus quasiperiodic attractor to SNA through the HH mechanism as shown in Figs. 3 and 4. It has been found that the simulated results and experimentally observed results in the phase-space as well as power spectra are qualitatively similar to each other. In particular, in both cases, the spectra of the quasiperiodic attractors are concentrated at a small discrete set of frequencies while the spectra of SNA have a much richer harmonic. To distinguish further in the characteristic aspect that the attractors depicted in Figs. 3, 4 & 6 are quasiperiodic and strange nonchaotic, we proceed to quantify the changes in the power spectrum. The spectral distribution (which is defined as the number

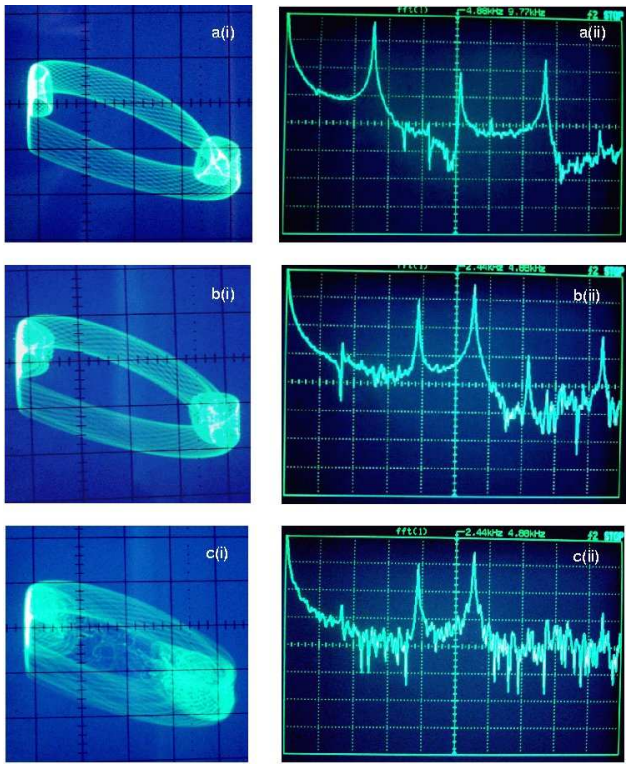


FIG. 6: (Color online) Attractors obtained experimentally from the circuit given in Fig. 1 corresponding to Figs. 4. (a) period-3 torus (3T) for R=2109 Ω, (b) period-6 torus (6T) for R=2106 Ω and (c) SNA at R=2104 Ω for fixed value of $E_{f1}$=0.22 V: (i) phase trajectory in the $(v - i_L)$ space; (ii) power spectrum.

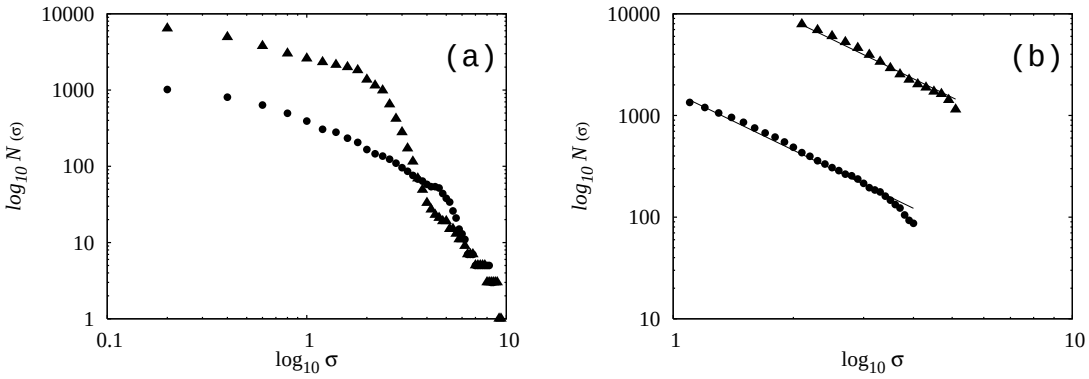


FIG. 7: Spectral distribution function for the quasiperiodic attractors and SNAs created through the Heagy-Hammel route: (a) quasiperiodic attractor, (b) strange nonchaotic attractor. Here the numerical study is indicated by filled circles, and experimental result is denoted by filled triangles.

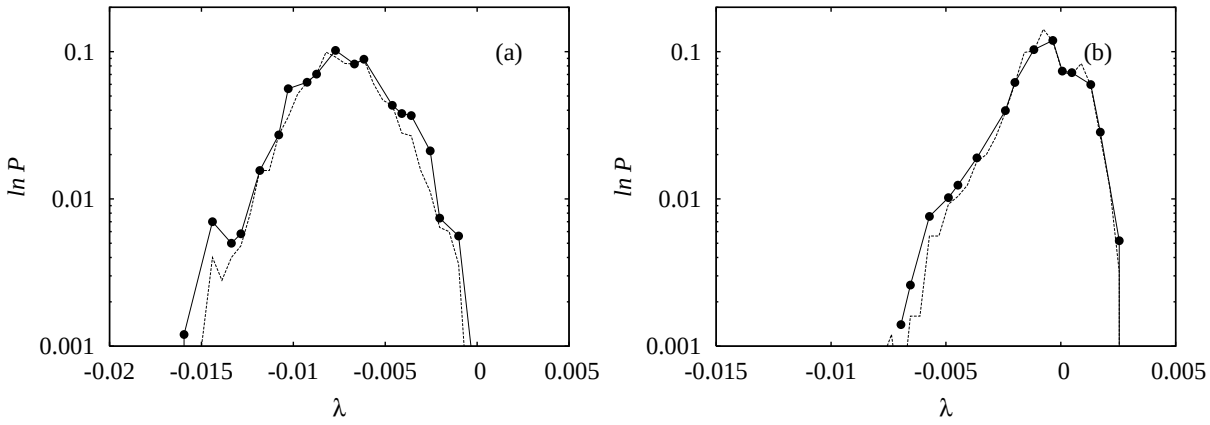


FIG. 8: Distribution of finite-time Lyapunov exponents on SNAs created through the Heagy-Hammel route: (a) quasiperiodic attractor, (b) strange nonchaotic attractor. Finite-time Lyapunov exponents calculated from numerical data are indicated by dashed lines, and from experimental data are denoted by solid lines.

of peaks in the Fourier amplitude spectrum larger than some value say $\sigma$) for quasiperiodic attractor and SNA are shown in Figs 7. In Figs. 7 the filled circles and the filled triangles denote the spectral distribution obtained through numerical simulation and experimental measurements respectively. The experimental data are recorded using a 16-bit data acquisition system (AD12-16U(PCI)EH) at the sampling rate of 200 kHz. It is found numerically as well as experimentally that the quasiperiodic attractors obey a scaling relationship $N(\sigma)$=$\log_{10}(1/\sigma)$ [see Fig. 7(a)] while the SNAs satisfy a scaling power law relationship $N(\sigma) = \sigma^{-\beta}$, $1 < \beta < 2$. The approximate straight line in the log-log plot shown in Fig. 7(b) obeys the power-law relationship with a value of $\beta = 1.9$ for numerical study and 1.84 for experimental study.

It has also been found that a typical trajectory on a SNA actually possesses positive Lyapunov exponents in finite time intervals, although the asymptotic exponent is negative. As a consequence, one observes the different characteristics of SNA created through different mechanisms by a study of the differences in the distribution of finite-time exponents $P(N, \lambda)$ [13]. For each of the cases, the distribution can be obtained by taking a long trajectory and dividing it into segments of length $N$, from which the local Lyapunov exponent can be calculated. In the limit of large $N$, this distribution will collapse to a $\delta$ function $P(N, \lambda) \longrightarrow (\delta - \lambda)$. The deviations from and the approach to the limit can be very differ-

ent for SNAs created through different mechanisms. We apply Wolf algorithm to determine the Lyapunov exponents from the experimental data [34]. Fig. 8 illustrates the distributions for $P(2000, \lambda)$ which is strongly peaked about the Lyapunov exponent when the attractor is a torus, but on the SNA the distribution picks up a tail which extends into the local Lyapunov exponent $\lambda > 0$ region. (Finite-time Lyapunov exponents calculated from numerical data are indicated by dashed lines, and from experimental data are denoted by solid lines) This tail is directly correlated with enhanced fluctuation in the Lyapunov exponent on SNAs. On Heagy-Hammel SNA, the distribution shifts continuously to larger Lyapunov exponents. Further the shapes for the torus regions [Fig. 8(a)] and SNA regions [Fig. 8(b)] are very different. The results clearly confirm that the HH mechanism is operative in the parameter regime of the present discussion.

## V. FRACTALIZATION ROUTE TO SNA

The second one of the routes we have identified in the present system is the gradual fractalization route where a torus gets increasingly wrinkled and then transits to a SNA without interaction (in contrast to the previous case of HH) with a nearby unstable orbit as we change the system parameter. In this route a period-$3^k$ torus becomes wrinkled and then the wrinkled attractor gradually loses its smoothness and forms a $3^k$-band SNA as we change the system parameter $a$ for fixed value of $E_1$. The qualitative (geometric) structure of the attractor remains more or less the same during the process. Such a phenomenon has been observed in the present circuit in two different regions indicated as F in Fig. 2 for certain ranges of $a$ in the regions of interest.

### A. Numerical Analysis

Now let us consider the phase diagram (Fig. 2) where we have identified such type of fractalization. To exemplify the nature of this transition, we fix the parameter $E_1$ at $E_1 = 0.34$, and vary $a$ in the range $0.953 < a < 0.955$ (Fig. 2). On decreasing the $a$ value, oscillations of torus (3T) in the amplitude direction starts to appear at $a = 0.954406$ (Fig. 9(a)) whose phase portrait and power spectrum are shown in Figs. 10a(i) and 10a(ii). As $a$ is decreased further to $a = 0.954351$, the oscillatory behavior of the torus gradually approaches a fractal

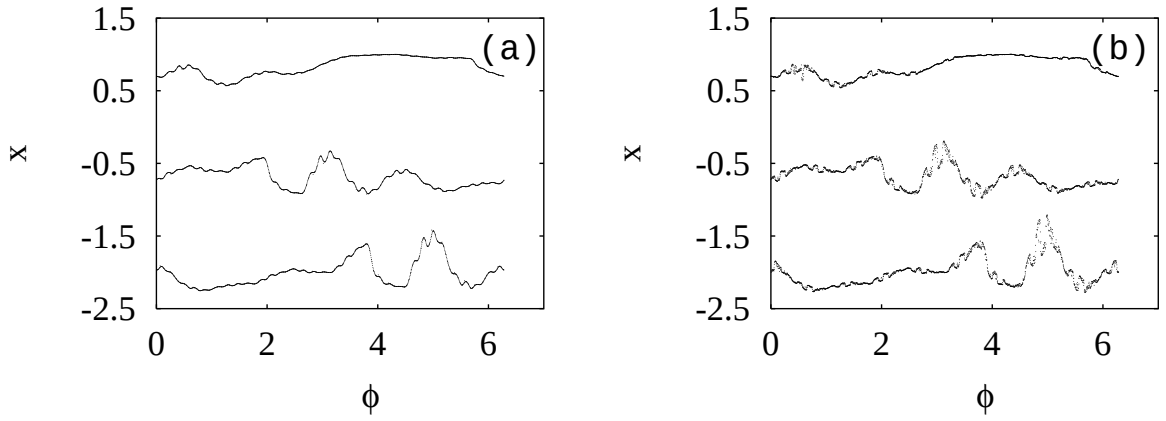


FIG. 9: Projection of the numerically simulated attractors of Eqs. (2) in the $(\phi - x)$ plane for fixed $E_1$ =0.34 and various values of $a$ indicating the transition from quasiperiodic attractor to SNA through fractalization route. (a) period-3 torus (3T) for $a$=0.954406 and (b) SNA at $a$=0.954351.

nature. The torus (3T) attractor gets increasingly wrinkled and transforms into a SNA at $a_{GF}$ = 0.954351 as shown in Fig. 9(b). The corresponding phase portrait and power spectrum are shown in Fig. 10b(i) and 10b(ii).

At such values, the nature of the attractor is strange (see Fig. 9(b)) eventhough the largest Lyapunov exponent in Fig. 11(a) remains negative. It is very obvious from these transitions that the 3 torus with three smooth branches in the Poincaré map (Fig. 9(a)) gradually losses its smoothness and ultimately approaches a fractal behavior via a SNA (in Fig. 9(b)) before the onset of chaos as the parameter $a$ decreases further. Such a phenomenon is essentially a gradual fractalization of the torus as was shown by Nishikawa and Kaneko [17] in their route to chaos via SNA. In this route, there is no collision involved among the orbits and therefore the Lyapunov exponent and its variance change only slowly as shown in Fig. 11(a) and 11(b) and there are no significant changes in its variance (see Fig. 10(b)). At even lower values of '$a$', $a$ = 0.954, the circuit exhibits chaotic oscillations as shown in region C of Fig. 2.

### B. Experimental confirmation

To confirm the numerical results further, experimentally measured phase portraits and Fourier spectrum results corresponding to the circuit of Fig. 1 are presented in Figs. 12

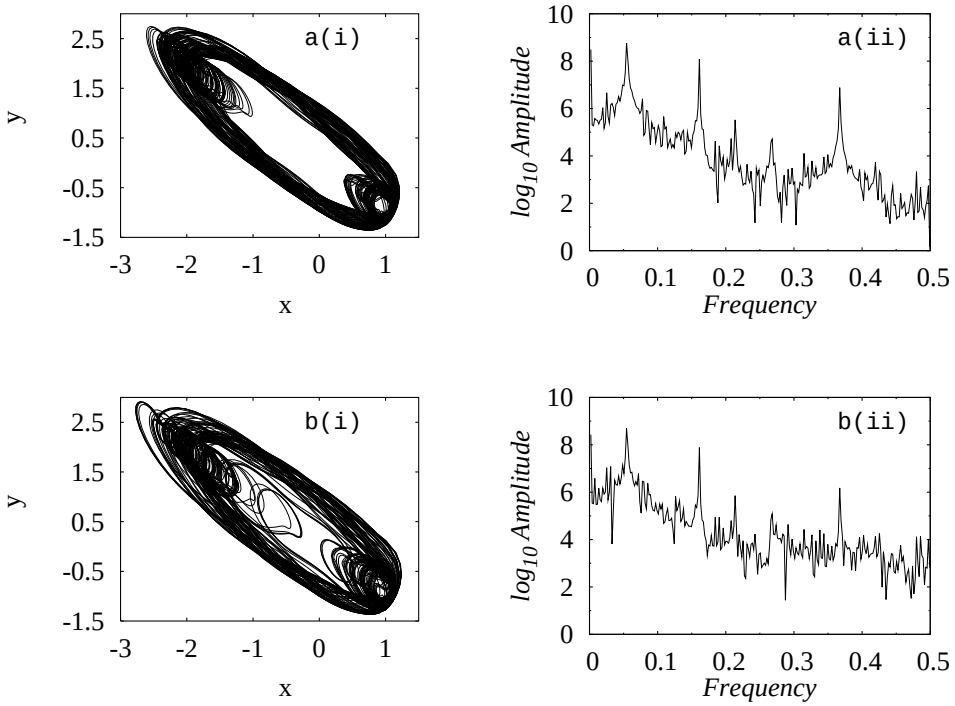


FIG. 10: Projection of the numerically simulated attractors of Eqs. (2) in the $(x, y)$ plane for fixed $E_1$ =0.34 and various values of $a$ indicating the transition from quasiperiodic attractor to SNA through fractalization route:(a) period-3 torus (3T) for $a$=0.954406 and (b) SNA at $a$=0.954351: (i) phase trajectory in the $(x - y)$ plane ; (ii) power spectrum.

which correspond to the transition from quasiperiodic attractor to SNA through gradual fractalization shown in Figs. 9 and 10. It has been noticed that the simulated results and experimentally measured results in the phase-space as well as power spectrum are in close agreement. To verify further whether the attractors depicted in Figs. 10 and 12 are quasiperiodic and strange nonchaotic attractors, we proceed to quantify the changes in the numerically and experimentally measured power spectra. In our analysis it has been verified that the quasiperiodic attractor obeys a scaling relationship $N(\sigma)$=$\log_{10}(1/\sigma)$[see Fig.13(a)] while in the approximate straight line shown in the log-log plot Fig. 13(b) satisfying the power relationship $N(\sigma) = \sigma^{-\beta}$, with an estimated value of $\beta$=1.78 for simulation and $\beta$=1.9 for experimental measurement confirms that the attractor created through this mechanism is indeed a strange nonchaotic attractor.

Fig. 14 illustrates the distributions for $P(2000, \lambda)$ which is strongly peaked about the Lyapunov exponent when the attractor is a torus, but on the SNA the distribution picks

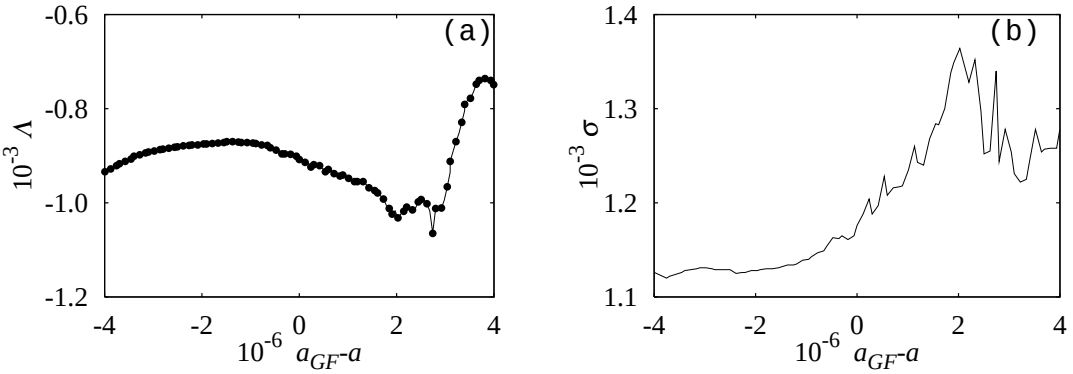


FIG. 11: Transition from three torus to SNA through fractalization route obtained from numerical data: (a) the behavior of the maximal Lyapunov exponent ($\Lambda$) and (b) the variance ($\sigma$) for $E_1$=0.34.

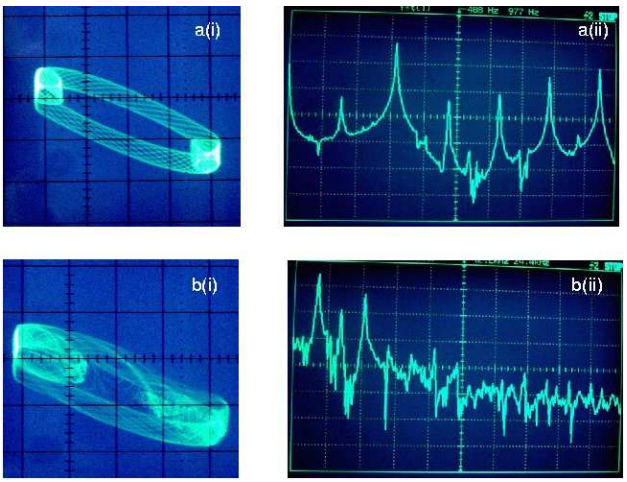


FIG. 12: (Color online) Attractors obtained experimentally from the circuit given in Fig.1 corresponding to Figs. 10. (a) period-3 torus (3T) for R=2102 Ω and (b) SNA at R=2101 Ω for fixed value of $E_{f1}$=0.17 V: (i) phase trajectory ($v - i_L$); (ii) power spectrum.

up a tail which extends into the local Lyapunov exponent $\lambda > 0$ region. This tail is directly correlated with enhanced fluctuation in the Lyapunov exponent on SNAs. On the fractalized SNA , the distribution shifts continuously to larger Lyapunov exponents, but the shape remains the same for torus regions as well as SNA regions.

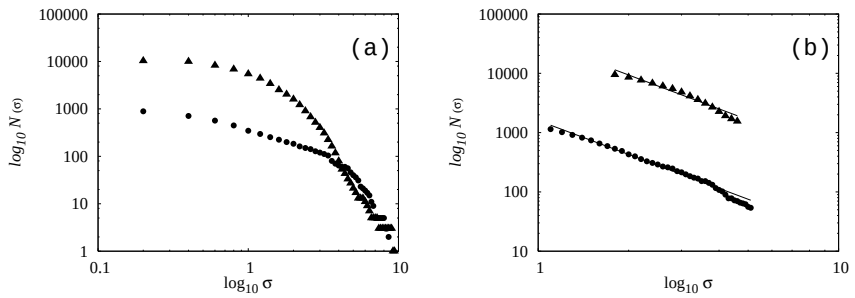


FIG. 13: Spectral distribution function for spectra of quasiperiodic attractor and SNAs created through gradual fractalization route: (a) quasiperiodic attractor, (b) strange nonchaotic attractor.Here numerical study is indicated by the filled circles and experimental study is denoted by the filled triangles.

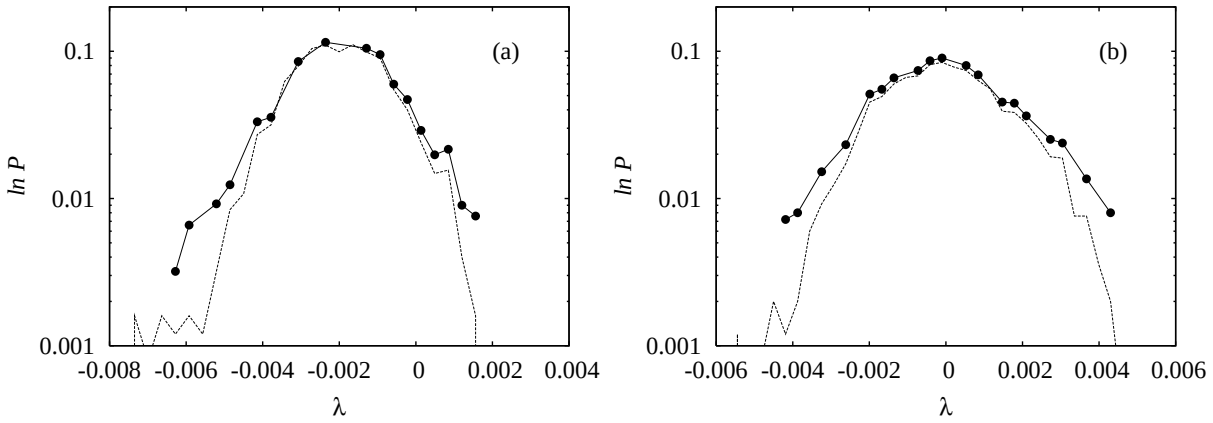


FIG. 14: Distribution of finite-time Lyapunov exponents on SNAs created through gradual fractalization.: (a) quasiperiodic attractor, (b) strange nonchaotic attractor. Finite-time Lyapunov exponents calculated from numerical data are indicated by dashed lines, and from experimental data are denoted by solid lines.

## VI. INTERMITTENT ROUTE TO SNA

Finally, the third of the routes that is predominant in this system is an intermittent route in which the torus is eventually replaced by a strange nonchaotic attractor through an analog of the saddle-node bifurcation. Such a phenomenon has been identified within the range $0.623 < E_1 < 0.645$ for the amplitude while the parameter $a$ is decreasing from right to left in the narrow range $0.949 < a < 0.954$ for fixed $E_1$.

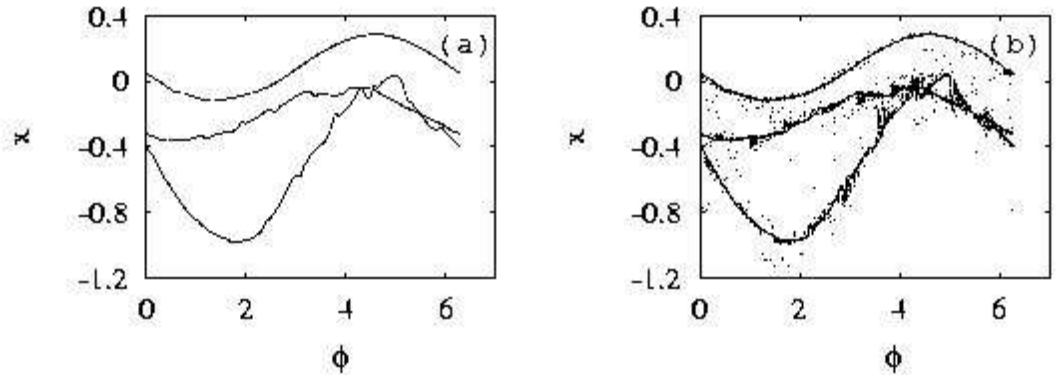


FIG. 15: Projection of the simulated attractors of Eqs. (2) in the $(\phi - x)$ plane for fixed $E_1$ =0.635 and various value of a: indicating the transition from quasiperiodic attractor to SNA through type I intermittent route. (a) torus (3T) for a=0.951912 and (b) SNA at a=0.951889.

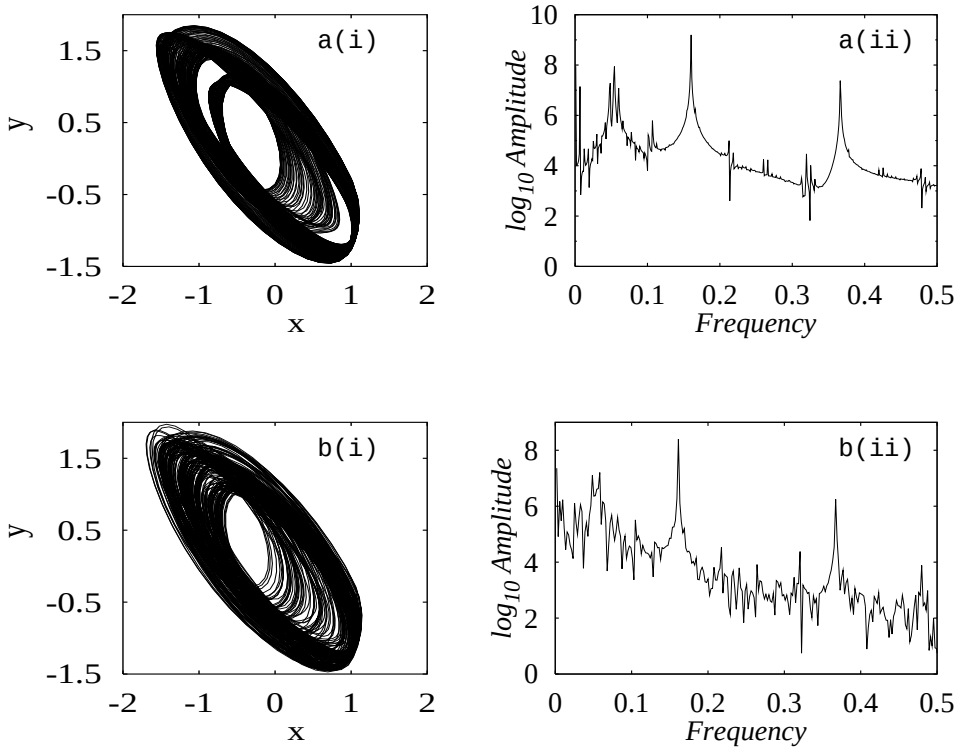


FIG. 16: Projection of the numerically simulated attractors of Eqs. (2) for fixed $E_1$ =0.635 and two different values of $a$ indicating the transition from quasiperiodic attractor to SNA through type I intermittent route: (a) period-3 torus (3T) for $a$=0.951912 and (b) SNA at $a$=0.951889: (i) phase trajectory in the $(x - y)$ plane; (ii) power spectrum.

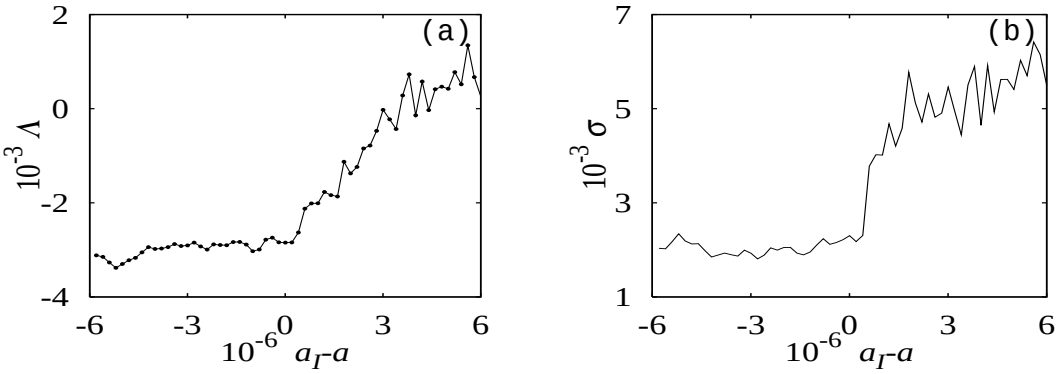


FIG. 17: Transition from three torus to SNA through type I intermittent mechanism obtained from numrical data: (a) the behavior of the maximal Lyapunov exponent ($\sigma$) and (b) the variance ($\Lambda$) for $E_1 = 0.635$.

### A. Numerical Analysis

To illustrate the above transition, let us fix the parameter $E_1$ at $E_1 = 0.635$ while $a$ is decreased from $a = 0.95192$. Figure 15(a) shows the projection of a three-period quasiperiodic attractor which has three smooth branches in the Poincaré section. The corresponding phase portrait and power spectrum are shown in Figs. 16a(i) and 16a(ii). As $a$ is decreased further, the attractor starts to wrinkle. On further decrease of $a = 0.951889$, the attractor becomes extremely wrinkled and has several sharp bends. However, as '$a$' passes a threshold value $a_I = 0.951876$, an intermittent transition from the torus to SNA occurs. At the intermittent transition, the amplitude variation loses its regularity and a burst appears in the regular phase (quasiperiodic orbit trajectory). The duration of laminar phases in this state is random. An example of the transition to such SNAs is shown in Fig. 15(b), the corresponding phase portrait and power spectrum are shown in Figs. 16b(i) and 16b(ii). At this transition, we also note that there is an abrupt change in the maximal Lyapunov exponent as well as its variance corresponding to the characteristic signature of the intermittent route [indicated in Figs. 17(a) and 17(b)] to SNA.

In the HH case, the points on the SNA are distributed over the entire region enclosed by the wrinkled bounding torus, while in the fractalization case the points on the SNA are distributed mainly on the boundary of the torus. Interestingly, in the present case shown in Fig. 15(b), most of the points of the SNA remain within the wrinkled torus with sporadic

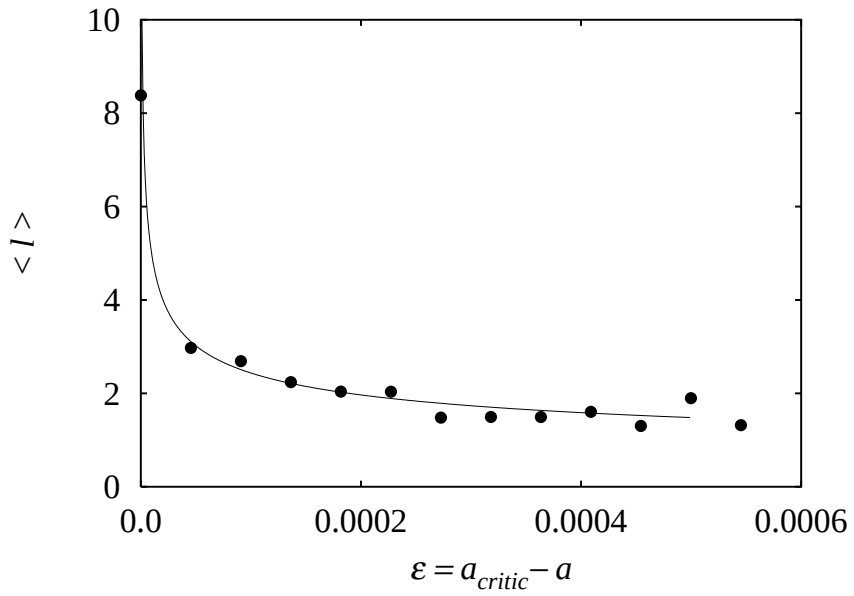


FIG. 18: Average laminar length ($< l >$) vs ($a_{critic} - a$) at $a_{critic} = 0.951876$ obtained from numerical data.

large deviations. The dynamics at this transition obviously involves a kind of intermittency. Such an intermittency transition could be characterized by scaling behavior. The laminar phase in this case is the torus while the burst phase is the nonchaotic attractor. In order to calculate the associated scaling constant, we coevolve the trajectories for two different values of $a$, namely, $a_c$ and another value of a near to $a_c$, while keeping identical initial conditions $(x_i, \theta_i)$ and the same parameter value $E_1$. As the angular coordinate $\theta_i$ remains identical, the difference in $x_i$ allows one to compute the average laminar length between the bursts. The plot of average laminar length $< l >$ for this attractor reveals a power law relationship of the form

$$< l >= (a_{\rm critical} - a)^{-\alpha}. \tag{3}$$

with the estimated value of $\alpha$ =0.31 (see Fig. 18). This analysis also confirms that such an attractor is associated with standard intermittent dynamics of type I described in Ref. [35, 36, 37].

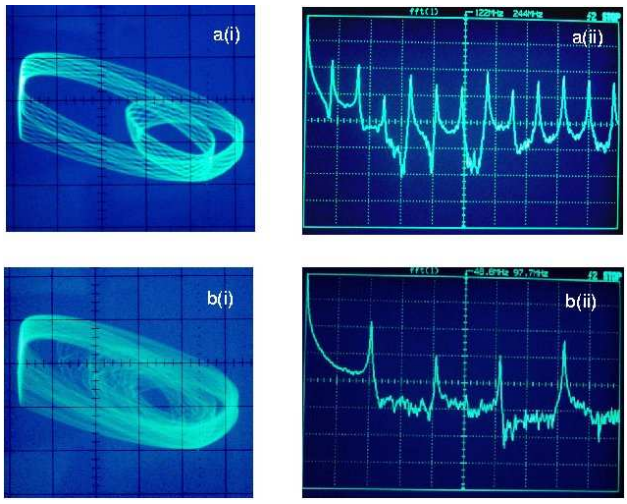


FIG. 19: (Color online) Attractors obtained experimentally from the circuit given in Fig.1 corresponding to Figs. 16. (a) period-3 torus (3T) for R=2099 Ω and (b) SNA at R=2097 Ω for fixed value of $E_{f1}$=0.318 V: (i) phase trajectory $(v - i_L)$; (ii) power spectrum.

### B. Experimental Confirmation

Next, we compare the simulation results in Figs. 16 and the experimental results given in Figs. 19. The range of parameters chosen for experimentally measured phase portraits and Fourier spectra results given in Figs. 19 correspond to the transition from quasiperiodic attractor to SNA through intermittent nature shown in Figs. 15 and 16. It has been found that the simulated results and experimentally observed results in the phase-space as well as power spectrum appears to be qualitatively similar in nature. To distinguish further that the attractors depicted in Figs. 15, 16 and 19 are quasiperiodic and strange nonchaotic attractors, the numerically and experimentally measured power spectra are quantified. It has been noted that the quasiperiodic attractor obeys a scaling relationship $N(\sigma)$=$\log_{10}(1/\sigma)$ [see Fig. 20(a)] while the SNAs created through this mechanism satisfy a scaling power law relationship $N(\sigma) = \sigma^{-\beta}$, $1 < \beta < 2$. The approximate straight line in the log-log plot shown in Fig. 20(b) obeys the power-law relationship with a value of $\beta = 1.86$ and 1.89 for numerical simulation and experimental measured studies respectively. Fig. 21 illustrates the distributions for $P(2000, \lambda)$ which is strongly peaked about the Lyapunov exponent when the attractor is a torus, but on the SNA the distribution picks up a tail which extends into the local Lyapunov exponent $\lambda > 0$ region. This tail is directly correlated with enhanced

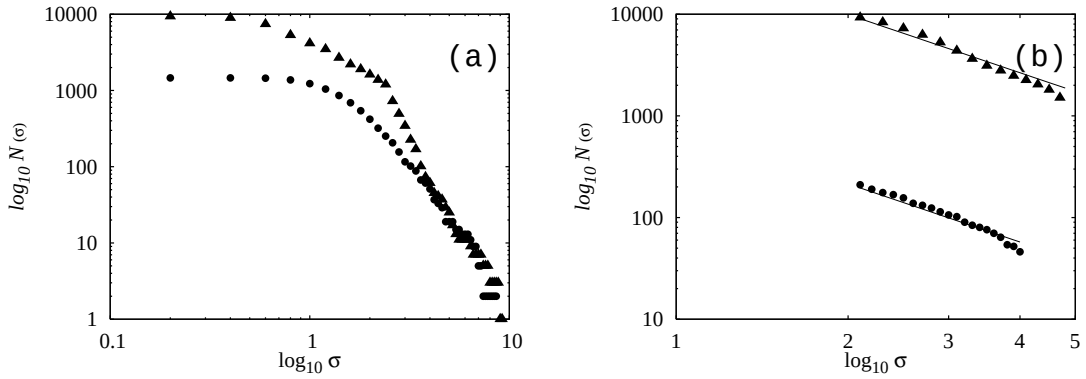


FIG. 20: Spectral distribution function for spectrum SNAs created through type-I intermittency route (circle denotes numerical study and triangle indicates experimental study).

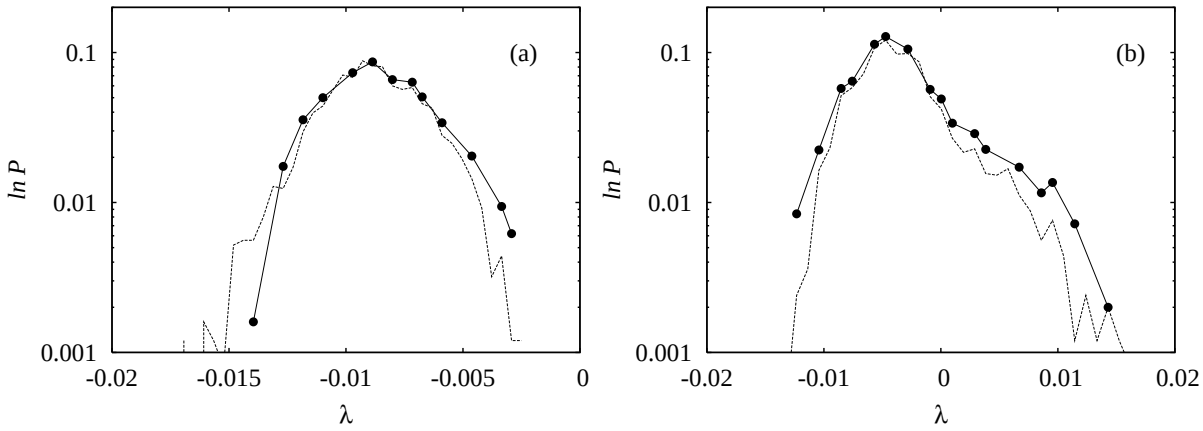


FIG. 21: Distribution of finite-time Lyapunov exponents on SNAs created through type-I intermittency. (a) quasiperiodic attractor, (b) strange nonchaotic attractor. Finite-time Lyapunov exponents calculated from numerical data are indicated by dashed lines, and from experimental data are denoted by solid lines.

fluctuation in the Lyapunov exponent on SNAs. On the intermittent SNA route, the actual shapes of distribution on the torus and the SNA are very different.

## VII. SUMMARY AND CONCLUSION

In this paper, various transitions from the quasiperiodic attractors to the strange nonchaotic attractors are demonstrated experimentally in a simple quasiperiodically driven electronic system. Specifically, the three prominent routes, namely Heagy-Hammel, fractaliza-

tion and type I intermittent routes for the creation of SNAs are demarcated the different regions in the $(a - E_1)$ parameter space. First, we have used simulation results to show the bifurcation process of this circuit from the quasiperiodic attractors to the strange nonchaotic attractors. Then we have experimentally observed the existence of the strange nonchaotic attractors as a part of the whole bifurcation process as predicted by the simulation. The experimental observations, numerical simulations and characteristic analysis show that the simple dissipative quasiperiodically forced negative conductance series LCR circuit does indeed have strange nonchaotic behaviors. To distinguish among the three mechanisms through which SNAs are born, we have examined the manner in which the maximal Lyapunov exponent and its variance change as a function of the parameters. In addition, we have also examined the distribution of local Lyapunov exponents and found that they take on different characteristics for different mechanisms.

Given the ubiquity of SNA dynamics in the quasiperiodically driven systems, one of the main issues with respect to the observation of SNAs is that this dynamical behaviour occurs in a very narrow range of values of the control parameters. While identifying these attractors from numerical analysis, one may wonder whether they occur due to numerical artifacts and whether they may get smeared out if the inherent noise or parameter mismatch is included. For this purpose, it is important to verify the underlying phenomena experimentally to be sure about the existence of the type of transitions to SNAs discussed in this paper. It is here the construction of electronic circuits like the one discussed in this manuscript gains physical relevance as an elegant means of experimental verification.

**Acknowledgments**

This work has been supported by a Department of Science and Technology, Government of India sponsored research project. The work of M. L was carried out under the DAE-BRNS Raja Ramana Fellowship Programme.

[1] C. Grebogi, E. Ott, S. Pelikan, and J. A. Yorke, Physica D **13**, 261 (1984).

[2] F. J. Romeiras and E. Ott, Phys. Rev. A **35**, 4404 (1987); F. J. Romeiras, A. Bondeson, E. Ott, T. M. Andonsen, Jr., and C. Grebogi, Physica D **26**, 277 (1987); Y. C. Lai, Phys. Rev. E **53**, 57 (1996); T. Nishikawa, and K. Kaneko, Phys. Rev. E **54**, 6114 (1996).

[3] A. Bondeson, E. Ott, and T. M. Antonsen, Jr., Phys. Rev. Lett. **55**, 2103 (1985).

[4] M. Ding, C. Grebogi, and E. Ott, Phys. Rev. A **39**, 2593 (1989); M. Ding and J. A. Scott Relso, Int. J. Bifurcation and Chaos Appl. Sci. Eng. **4**, 533 (1994).

[5] J. F. Heagy and W. L. Ditto, J. Nonlinear Sci. **1**, 423 (1991); J. I. Staglino, J. M. Wersinger, and E. E. Slaminka, Physica D **92**, 164 (1996).

[6] T. Yalcinkaya and Y. C. Lai, Phys. Rev. Lett. **77**, 5039 (1996).

[7] T. Kapitaniak and J. Wojewoda, *Attractors of Quasiperiodically Forced Systems* (World Scientific, singapore, 1993).

[8] A. Venkatesan, M. Lakshmanan, A. Prasad, and R. Ramaswamy, Phys. Rev. E **61**, 3641 (2000).

[9] A. Venkatesan and M. Lakshmanan, Phys. Rev. E **55**, 5134 (1997); A. Venkatesan and M. Lakshmanan, Phys. Rev. E **58**, 3008 (1998).

[10] T. Yang and K. Bilimgut, Phys. Lett. A **236**, 494 (1997).

[11] Z. Liu and Z. Zhua, Int. J. Bifurcation and Chaos Appl. Sci. Eng. **6**, 1383 (1996); Z. Zhua and Z. Liu, idbi **7**, 227 (1997).

[12] A. Venkatesan, K. Murali, and M. Lakshmanan, Phys. Lett. A **259**, 246 (1999).

[13] A. Prasad, V. Mehra, and R. Ramaswamy, Phys. Rev. Lett. **79**, 4127 (1997); Phys. Rev. E **57**, 1576 (1998).

[14] A. S. Pikovsky and U. Feudel, Chaos **5**, 253 (1995); U. Feudel, J. Kurths, and A. S. Pikovsky, Physica D **88**, 176 (1995).

[15] A. S. Pikovsky and U. Feudel, J. Phys. A **27**, 5209 (1994); S. P. Kuznetsov, A. S. Pikovsky, and U. Feudel, Phys. Rev. E **51**, R1629 (1995); A. Witt, U. Feudel, and A. S. Pikovsky, Physica D **109**, 180 (1997).

[16] V. S. Anishchenko, T. E. Vadivasova, and O. Sosnovtseva, Phys. Rev. E **53**, 4451 (1996); O. Sosnovtseva, U. Feudel, J. Kurths, and A. S. Pikovsky, Phys. Lett. A **218**, 225 (1996); S.

Kuznetsov, U. Feudel, and A. Pikovsky, Phys. Rev. E **57**, 1585 (1998).

[17] T. Nishikawa and K. Kaneko, Phys. Rev. E **54**, 6114 (1996).

[18] A. Venkatesan and M. Lakshmanan, Phys. Rev. E **63**, 026219 (2001).

[19] B. R. Hunt and E. Ott, Phys. Rev. Lett. **87**, 254101 (2001); J. W. Kim, S. Y. Kim, B. Hunt, and E. Ott, Phys. Rev. E **67**, 036211 (2003).

[20] S. Y. Kim, W. Lim, and E. Ott, Phys. Rev. E **67**, 056203 (2003).

[21] W. Lim and S. Y. Kim, J. Korean Physical Society **3**, 514 (2004).

[22] J. F. Heagy and S. M. Hammel, Physica D **70**, 140 (1994).

[23] W. L. Ditto, M. L. Spano, H. T. Savage, S. N. Rauseo, J. Heagy, and E. Ott, Phys. Rev. Lett. **65**, 533 (1990).

[24] T. Zhou, F. Moss, and A. Bulsara, Phys. Rev. A **45**, 5394 (1992).

[25] W. X. Ding, H. Deutsch, A. Dinklage, and C. Wilke, Phys. Rev. E **55**, 3769 (1997).

[26] J. A. Ketoja and I. Satija, Physica D **109**, 70 (1997).

[27] A. Prasad, R. Ramaswamy, I. I. Satija, and N. Shah, Phys. Rev. Lett **83**, 4530 (1999).

[28] C. S. Zhou and T. L. Chen, Europhys. Lett. **38**, 261 (1997).

[29] R. Ramaswamy, Phys. Rev. E. **56**, 7294 (1997).

[30] R. Chacon and A. M. Gracia-Hoz, Europhys. Lett. **57**, 7 (2002).

[31] S. Y. Kim and W. Lim, J. Phys. A **37**, 6477 (2004).

[32] T. Kapitaniak and L. O. Chua, Int. J. Bifurcation and Chaos Appl. Sci. Eng. **7**, 423 (1997).

[33] K. Thamilmaran, D. V. Senthilkumar, M. Lakshmanan, and A. Ishaq Ahmed, Int. J. Bifurcation and Chaos Appl. Sci. Eng. **15**, 2 (2005).

[34] A. Wolf, J. B. Swift, H. L. Swinney, and A. W. John, Physica D **16**, 285 (1985).

[35] Y.Pomeau and P. Manneville, Commun. Maths. Phys. **74**, 1891 (1980).

[36] M. Lakshmanan and S. Rajasekar, *Nonlinear Dynamics: Integrability, Chaos and Pattern Formation* (Springer-Verlag, Berlin, 2003).

[37] E. Ott, *Chaos in Dynamical Systems* (Cambridge University Press, Cambridge, 1994).